BULLETIN OF THE POLISH ACADEMY OF SCIENCES
TECHNICAL SCIENCES, Vol. 72(5), 2024, Article number: e150808
DOI: 10.24425/bpasts.2024.150808



# Performance evaluation of 5G New Radio low-density parity check codes over different scenarios of lognormal fading channel

**Mohammed Hussein ALI*** and **Ghanim A. AL-RUBAYE**

Electrical Engineering Department, College of Engineering, Mustansiriyah University, Baghdad, Iraq

**Abstract.** Low-density parity check (LDPC) is a channel coding technique widely utilized in the 5G New Radio standard, it is of utmost importance in facilitating proficient and secure communication in noisy environments by effectively minimizing errors during data transmission. It is primarily used in the 5G New Radio (NR) standard for encoding user information on the physical downlink shared channel (PDSCH). The necessity to satisfy the increasing expectations for throughput, latency, and dependability led to the decision to deploy LDPC codes for user data, especially in the enhanced mobile broadband (eMBB) and ultra-reliable and low-latency communications (URLLC) scenarios of 5G networks. The present system proposes the use of NR-LDPC codes to transmit data across a lognormal multipath fading channel model in the presence of AWGN. Wireless communication channels often use a lognormal multipath fading channel model, where the received signal experiences both multipath fading and lognormal shadowing. The research investigates the effectiveness of NR-LDPC coding in improving QAM-OFDM system performance by analyzing two rate-compatible base graphs and comparing their effectiveness with an uncoded system. This analysis is crucial for optimizing communication network design, especially in scenarios where the integrity of data is of utmost importance. We introduce a new method to improve the 5G NR LDPC code capability under lognormal fading conditions. This approach develops a layered min-sum (LMS) algorithm to provide enhanced error-correcting capabilities. The developed and implemented decoding algorithm represents a significant advancement over traditional detection methods. The outcomes of the simulation provide evidence of the effectiveness of the proposed NR-LDPC coding techniques in terms of their error correction and identification capabilities. In addition, the developed LMS decoding algorithm was shown to significantly decrease the BER of the system.

**Keywords:** QAM; OFDM; NR-LDPC; lognormal fading channel; BER; 5G NR; physical uplink shared channel (PUSCH); physical downlink control channel (PDCCH); enhanced mobile broadband (eMBB); LTE-advanced (LTE-A).

## 1. INTRODUCTION

Wireless communications of the 5G are estimated to provide for a variety of scenarios. Wireless communication in high mobility conditions, such as fast-speed railroads and unmanned aerial vehicles (UAVs) drones, is considered a critical situation. Nevertheless, the significant mobility frequently results in substantial Doppler shift, hence posing significant challenges to the reliability of wireless communications. Various strategies have been explored to facilitate high-mobility communications. The coding of channels is a core part of any communication network. Future wireless systems will require powerful algorithms with low-complexity encoding and decoding to meet a wide variety of requirements, from running in highly dependable situations with simple informational messages along with low coding rates for operating in situations requiring high throughput, long messages, and high coding rates. Utilizing, low-density parity check (LDPC) codes is mostly seen in the physical downlink shared channel (PDSCH) of the Fifth Generation New Radio (5G NR) standard [1]. The selection of LDPC codes algorithm for client data and utilization of Polar codes for control data, particularly in the context of enhanced mobile broadband (eMBB), and ultra-reliable low latency communications (URLLC) scenarios, was motivated by the objective of achieving the demands for enhanced throughput, reduced latency, and are known for their robust error-correcting capabilities and are highly suitable for scenarios with high data flow, such as eMBB. The ability to accurately resolve inaccuracies in the received data significantly contributes to guaranteeing the dependable transfer of user data through the PDSCH.

LDPC codes have significance for ensuring fast and reliable communication in a noisy channel environment because they aid in lowering data transmission errors. An earlier version of the LDPC code was first presented in [3] and has undergone extensive development over many decades. It has found significant use in several wireless communication contexts, including profound space communications [4], digital terrestrial TV broadcasting (DTTB) [5–8], and wireless local area networks (WLANs) [9]. One of the major technological advances in 5G NR is the introduction of LDPC code utilized for channel coding technique for the data channel, where Turbo coding that was used in Fourth Generation Long Term Evolution (4G LTE) and Long Term Evolution – Advanced (LTE-A) networks is now replaced [4]. Orthogonal frequency division multiplex-

*e-mail: eeph005@uomustansiriyah.edu.iq

Manuscript submitted 2024-03-30, revised 2024-06-02, initially accepted for publication 2024-06-03, published in September 2024.

ing (OFDM) is a widespread modulation technique utilized by wireless communication networks. The operational approach is the division of an extremely fast data stream into many streams with reduced data rates. These streams are then sent simultaneously using a set of closely spaced subcarriers. OFDM is well recognized for its ability to diminish the negative impacts of interference from multiple directions and frequency-selective fading, making it a wise option for achieving high speeds of data transfer in diverse wireless communication technologies, such as 5G. The use of NR-LDPC-coded OFDM in the area of 5G and Beyond Fifth Generation (B5G) integrates the advantageous features of OFDM modulation with LDPC coding, hence enhancing error correction capabilities. In challenging wireless scenarios, this technology facilitates the achievement of high data transmission rates, reduced latency, and reliable connectivity. Comparing the LDPC codes to other iterative codes like turbo codes, they are fundamentally simpler and provide a fully parallelizable decoding implementation [10]. In general, turbo codes (TCs) contain complicated code structures, a significant delay in the decoding process, and other characteristics that make TCs inappropriate for 5G. LDPC codes provide superior performance and need less bandwidth, particularly when used to longer block lengths. According to reference [11, 12], LDPC codes exhibit higher efficiency compared to other coding schemes. Iterative soft-decision decoding of LDPC codes provides performance that is almost equivalent to the Shannon limit. Additionally, it offers reduced decoding complexity and allows for simple modification of code rates, resulting in improved BER performance compared to turbo codes [13].

Recently, a lot of approaches have been used to improve the error correction performance of 5G LDPC codes [14–19]. The modified minimum sum (MS) and algorithms that provide an extended approximation to the minimum value were introduced by [14] and then [15] by considering the approximate-min approach as described in reference [16]. The author in [17], improves the performance of the 5G NR system by employing the MS approach on the base matrix ($BG1$) within the decoder for LDPC, specifically focusing on 5G standards, and increasing iterations, especially for larger code words. A significant level of implementation complexity is required for non-linear functions like BP decoding. To streamline the non-linear functions inside the BP approach, a hybrid decoding methodology was introduced by the researchers in [18]. To enhance the precision of the calculations, the authors mentioned in [19] include offset and normalization factors in the decoding process at certain intervals. These variables are carefully adjusted using machine learning methods. Layered decoding algorithms may be used with normalized min-sum (NMS) or offset min-sum (OMS) algorithms to achieve an optimal equilibrium between BER, decoding complexity, and decoding convergence time [20].

Optimal use of the available spectrum may be achieved by the implementation of the OFDM communication technology. In this particular configuration, the usage of the spectrum may be significantly enhanced by using M-ary quadrature amplitude modulation (M-QAM). Nevertheless, in some scenarios, the use of high-order modulation techniques may result in a significant increase in error rates for low-power transmission systems. Forward error correction (FEC) is often used in the OFDM technique to diminish the occurrence of errors [21, 22]. OFDM is typically used in combination with a cyclic prefix (CP) to remove inter-symbol interference (ISI), which transforms frequency-selective channels into narrow-band frequency-flat fading channels.

In our research, we developed and implemented an NR-LDPC-QAM-OFDM system, and subsequently evaluated and compared its bit error rate (BER) performance with that of uncoded QAM-OFDM systems over a multipath lognormal environment and in an additive white Gaussian noise (AWGN). The findings of our research indicate that the NR-LDPC-COFDM system exhibits superior performance compared to the uncoded OFDM system in a multipath channel scenario characterized by progressive channel degradation. The LPDC-OFDM convergence requires a larger number of iterations, which is considered a significant limitation. On the other hand, the NR-LDPC technique can reduce the necessary decoding iterations for correcting channel errors by around 18-29% at a moderate signal-to-noise ratio. This article presents a comprehensive examination of the computation of BER in the context of a lognormal fading channel (LFC). The LFC is a commonly used theoretical framework within the domain of wireless communication systems. It is crucial to comprehend the BER achievement inside such channels to develop communication systems that are both dependable and efficient.

The subsequent parts of the article are organized according to the following structure: Section 2 of the LDPC code provides a comprehensive contextual foundation by demonstrating the techniques in more detail. This portion of the article explains the 5G NR LDPC code system.

Section 3 details the NR-LDPC-COFDM system design and implementation framework of the system. The computation of BER involves evaluating the error probability for each sent bit, taking into account the channel characteristics and the modulation scheme used within Section 4, while Section 5 provides a quantitative evaluation of LDPC-COFDM systems, presenting simulation results as empirical evidence of their performance. The last section of the paper summarizes the findings and implications.

## 2. 5G NR LDPC TECHNIQUES

Every possible channel in the physical world introduces unwanted noise, which in turn causes errors and lowers the system dependability. Channel coding improves the dependability of wireless communication networks by adding redundancies to transmit information in an organized manner. One subclass of linear block codes is LDPC codes, denoting that their whole specification may be determined just via their generating matrix G and H which is parity matrix H. The sparsity of these codes is one noteworthy feature, characterized by a reduced quantity of elements that are non-zero inside the H [23].

The codes from the LDPC process may be categorized into two separate groups: regular and non-regular. The popularity of LDPC code has increased significantly as a result of its ability

to achieve large throughputs, reduced decoding complexity, and better decoding latency. This is specifically advantageous within the framework of handling information with 5G technology. The protograph architecture used by the 5G-NR specifications encompasses many crucial aspects. Two basic graphs are available, namely $BG1$ as well as $BG2$ [24]. Various modifications such as $Z_C$, and techniques including shortening and puncturing to achieve various rates [25,26]. In the context of the 5G standard, a protograph is often denoted by a base graph structure [27]. The usage of a system is determined by either the coding rate or the quantity of information bits. The size of the transport block being transferred over the PDSCH determines which base graph is used, with $BG1$ of a size of $(46\times68)$ being when the size of the transit block surpasses a certain threshold, and $BG2$ of a dimension $(42\times52)$ being employed when the transfer block size is below this threshold. The $BG2$, being smaller in size, is considered more appropriate for shorter transport blocks due to its ability to strike a more favorable balance between complexity and efficiency.

The first ten columns of $BG1$ have a total of twenty-two information bits, whereas the first ten columns of $BG2$ contain ten data bits. It is crucial to consider the initial pair of columns for both $BGs$ are consistently perforated and do not engage in any activity in the transmission process. The generation of H of protograph codes may be achieved by replacing every zero-valued component of the $BG$ with a $(Zc\times Zc)$ all zero matrix and substituting every component has a value of zero by a $(Zc\times Zc)$ matrix of permutations. The term "lifting size", denoted as $Zc$, pertains to the number of attached copies of the protograph [28]. A total of 51 distinct lifting sizes have been specified. The variable $Zc$ is typically used to represent this concept, and its value can be determined by employing equation (1) with the given index and the maximum value provided by the $Z_c$ is 384 as shown in equation (1) [29,30]

$$Z_c = d\times 2^{i_{Ls}}. \tag{1}$$

The index $i_{LS}$ ranges from 0 to $I_d$, while $d$ is a number selected from the set (2, 3, 5, 7, 9, 11, 13, 15), and the value of $I_d \in$ (7, 7, 6, 5, 5, 5, 4, 4). which value is determined based on the index number (0, 1, 2, 3, 4, 5, 6, 7). One of the main benefits of utilizing a matrix of identities with a cyclic shift as a PM (permutation matrix) is that it allows each permutation to be represented by a single integer.

### 2.1. 5G NR LDPC encoder

The LDPC of $(NK)$ code is composed of a codeword with a length of $N$ bits, a message length of $K$ bits, and $(N-K)$ parity bits. The LDPC matrix, denoted as H, is a sparse matrix with dimensions $(N-K)*N$, where $N*(N-K)$ is the formula for calculating the overall number of entries. The use of two distinct base graphs throughout the encoding process serves the purpose of accommodating varied code rates. The primary use of the $BG1$ is for accommodating greater lengths of user data blocks within the 500–8448 range. Additionally, it is utilized to enable a very high rate of code variation, ranging from 1/3 to 8/9. The $BG2$ is utilized for short lengths of user data within the 40 to 2560 range, which is considered appropriate for lower variable rates ranging from 1/5 to 2/3 [31,32].

The data on the traffic channel is encoded by the LDPC coder by extending the message bits with parity bits. To ensure the safety of the data, a cyclic redundancy check (CRC) encoder segments the data into smaller blocks and attaches a CRC to each one. Rate-matching procedures might include either puncturing or shortening as shown in Fig. 1. The technique of encoding the LDPC code relies heavily on the H that is expanding upon the base matrix. The encoder is responsible for calculating the parity bits using a matrix operation. Lengths $K$, $N-K$, and $N$ of the array vector are, message $m = m_1, m_2, \ldots, m_K$ parity $p = p_1, p_2, \ldots, p_{(N-K)}$ and codeword $C = C_1, C_2, \ldots, C_{(N-K)}$.

The codeword $C$ that may be typed by equation (2) contains both the information and the computed parity:

$$C = m_1, m_2, \ldots, m_K, p_1, p_2, \ldots, p_{(N-K)}. \tag{2}$$

To get the correct codeword, which includes the data and specifies the process conducted on the data portion to compute the parity bits $(p)$, the H and codeword must meet equation (3):

$$[H] * \left[C^T\right] = 0. \tag{3}$$

The preceding equation may be simplified to equation (4) by decomposing the $H$ into its $P$ component and its $I$ identity component:

$$\begin{bmatrix} P & I \end{bmatrix} \begin{bmatrix} m^T \\ P^T \end{bmatrix} = 0. \tag{4}$$

The complex doubling diagonal matrix of the $H$ is used to identify the first four parity bits in the 5G standard, whereas the $I$ of the $H$ is utilized to determine the fifth and terminal parity bits.

### 2.2. 5G NR LDPC decoder

Due to its simple implementation and straightforward decoder, LDPC codes operate near their maximum capacity. Since the LDPC decoders employ soft-in soft-out (SISO) algorithms, the information sent by the decoders is a probability of the actual channel data that are received. The message is frequently delivered through the check nodes (CNs) and the variable nodes (VNs) via the SISO decoder. The decoder employs an iterative approach to estimate the actual values of the channel, bits one by one, based on the received vector. It utilizes the full incoming vector together with information from the bit that was previously decoded to estimate the subsequent bits. The internal transmission of information is facilitated by utilizing the LLR [33].

At the first iteration, the LDPC decoder utilized the intrinsic information of the channel, and intrinsic information was calculated for each of the received values independently, which corresponded exactly to the received value of the AWGN channel [34]. The LLR value can be determined as equation (5):

$$Li = \log\left(\frac{P_r\left(c_i = \dfrac{0}{y_i}\right)}{P_r\left(c_i = \dfrac{1}{y_i}\right)}\right) = \log\left(\frac{g\left(\dfrac{y_i}{c_i} = 0\right)}{g\left(\dfrac{y_i}{c_i} = 1\right)}\right) = \log\left(\frac{e^{2y_i}}{\sigma^2}\right), \tag{5}$$

where $Li$ represents LLR intrinsic information, which is initial knowledge or belief about the bits to be decoded. $c_i$ represents the $i^{th}$ bit of [C] while $y_i$ represents the $i$-th bit of received value. After being simplified, equation (5) yields the ultimate $Li$ value, as seen in equation (6):

$$Li = y_i * \left(\frac{2}{\sigma^2}\right). \tag{6}$$

The extrinsic LLR ($L_e$) output provides the belief of specific bits inside the incoming vector y. The use of the term "afterword" after the first iteration in the decoder of LDPC is feasible, as shown by equation (7):

$$L_e = \log\left(\frac{e^{[2*(y_1+y_2+y_3+\ldots+y_N)]}}{\sigma^2}\right), \tag{7}$$

where $y = \{y_1, y_2, y_3, \ldots, y_N\}$ represents the whole received vector, by eliminating the exponential term using logarithm

$$L_e = (y_1 + y_2 + y_3 + \ldots + y_N)\left(\frac{2}{\sigma^2}\right). \tag{8}$$

The term $\left(\frac{2}{\sigma^2}\right)$ is a positive factor and may be disregarded. Utilizing the (tanh) function, one may effectively express the calculation of the conditional $L_e$ immediately after the application of the expectation operation in iterative decoding algorithms, such as turbo codes, as in equation (9):

$$g(x) = \log\left(\tanh\left(\frac{|x|}{2}\right)\right). \tag{9}$$

An accurate way to estimate the final result of a log(tanh) function is to use a basic min-sum algorithm:

$$g(x, y) = \text{sign}(x) * \text{sign}(y) * \min(|\boldsymbol{x}|, |\boldsymbol{y}|). \tag{10}$$

The rows of the parity check matrix (PCM) are partitioned into multilayers using the layered min-sum technique [35–37], also known as layering. The process of layering is executed in a manner that ensures that each layer in the PCM has a column weight of one. The layered min-sum decoder (LMND) achieves superior error performance and requires fewer iterations, while also exhibiting more rapid convergence. As shown in Fig. 1, the initial decoder utilized the LLR for the first iteration and then applied the $L_e$ in subsequent iterations. The LMND employs an iterative process in which the decoders of each layer take turns updating the belief, and the final decoder makes an estimate based on the updated belief to produce the estimated decision. Subsequently, as the initial step in the process of layering, matrices are generated for each respective set. The two layers:

$$\text{H} = \begin{bmatrix} H_1 \\ H_2 \end{bmatrix} \quad \text{then} \quad L = \begin{bmatrix} L_1 \\ L_2 \end{bmatrix}.$$

In the initialization stage as the second step, the vector $y_j$ is utilized to modify the matrix $L_1$

$$L_1[:, j] = y_j \quad \text{for} \quad L_1[:, j] \neq 0,$$

where $j = 1, 2, \ldots, N$.

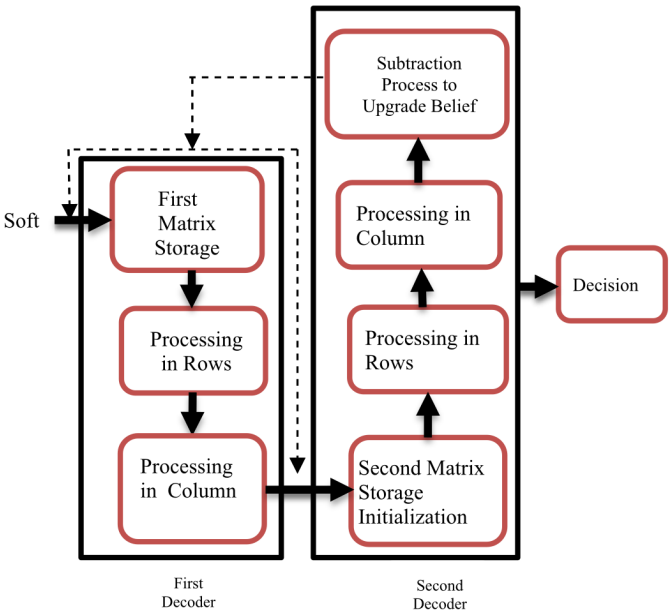


**Fig. 1.** Layered min-sum decoder

Following the initialization step, a min-sum (MS) method utilized the single parity check (SPC) algorithm for the decoder to carry out a row operation on each row of the PCM.

This task required the identification of the two smallest values, min1, and min2, as well as the determination of the location of min1 in the vector "POS". The sum of all the values in the $y_j$ vector is computed, referred to as parity ($P$). The aforementioned procedure is executed on the CNs inside the $\mathscr{L}$ matrix:

$$L_{[:,1:j]} = \min_2 \qquad \text{when} \quad L[i, j] \neq 0,$$
$$L_{[:,\text{Pos}]} = \min_1 \qquad \text{when} \quad L[i, j] \neq 0,$$
$$\text{the sign of} \quad L_{\text{New}} = L(\text{sign}) * P.$$

In the next step, the MS approach utilizes the repetition code to construct a new vector utilizing addition for each column of the PCM. The VNs are updated by performing the following column process assisted by the matrix $L$ and the whole vector $y_j$ to adjust the belief:

$$S_j = y_j + S(L_1[:, j]).$$

The sign of $L_{\text{New}} = L(\text{sign}) * P$.

Then executed a column operation on $L_2$

$$S_j = y_j + S(L_2[:, j]).$$

Update the summation of the variable $S_j$ from the first level of the given data set $L_1$

$$S_j = S_j - S(L_1[:, j]).$$

Update the summation of the variable $S_j$ from the first level of the given data set $L_2$

$$S_j = S_j - S(L_2[:, j]).$$

Finally, by utilizing a hard decision, the min-sum strategy predicts the ultimate codeword at a threshold of zero

$$d_k = g(x) = \begin{cases} 0, & S_j > 0, \\ 1, & S_j < 0. \end{cases} \tag{11}$$

From one decoder to another, the "enhancement of the subtract-min-sum algorithm" process is carried out via the LMS algorithm. The LMS technique exhibits an equilibrium between computational speed as well as effectiveness as a result of suboptimal stacking implementations.

## 3. 5G NR LDPC-COFDM SYSTEM MODEL

The architecture of our 5G NR LDPC-COFDM system is shown in Fig. 2. In the subsections that follow, we will break down the main parts of the system block diagram and explain what it does.

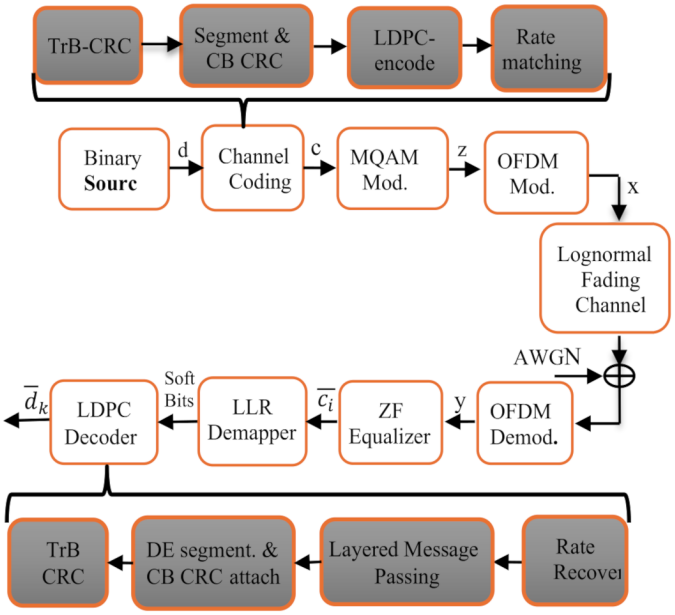


**Fig. 2.** Schematic structure NR-LDPC Code QAM-OFDM

### 3.1. Transmitter

The system transmitter con comprises an LDPC encoder, an M-QAM modulator, an inverse fast fourier transform (IFFT) portion, and a CP block. The input is supposed to have a perfectly random and statistically independent order of bits.

The input sequence of bits $(d = d_0, d_1, \ldots, d_{k-1})$ is encoded by utilizing an LDPC code. Both capacity-approaching codes have the same encoding rate of 0.5 and 0.333. The output of the NR-LDPC encoder $(c_i = c_0, c_1, \ldots, c_{n-1})$, is sent into a digital modulator, where it is rearranged into various patterns, such as the 4-QAM format, where two coded bits are merged to make a single symbol. One 16-QAM symbol is generated by combining four groups of coded bits. Under the gray mapping constellation, the bits that are coded are joined to create the matching symbol, therefore, the appropriate QAM symbol for a K-tuple $\{c_m, c_{m+1}, \ldots, c_{m+k+1}\}$ of bits, is:

$$X_k = \mathbf{C}\left[\sum_{m=0}^{k-1} 2^{k-1-m} c_m\right]. \tag{12}$$

The symbol $\mathbf{C} \in \mathbb{C}^{1\times 2^k}$ represents the vector of Gray-encoded in the time domain. Using a mapping to M symbols, the rate-matched bits of information are partitioned into collections of $m = \log 2(M)$ bits. Mapping points of constellations may be utilized to create symbols of QAM with length $N = E/m$. A serial-to-parallel converter receives the digitally modulated symbol of code bits $c_i$ and makes it possible to process the symbols $c_i$ in parallel and serially. The frequency domain is therefore represented by the symbol $c^f[\mathrm{i}]$ where $i = 1, 2, \ldots$ When an IFFT is applied, the signal that comes out is the time domain signal that corresponds to $c^t[i]$ to facilitate transmission, and the parallel signal is $c^t[i]$ returns to its serial form after conversion.

An N-points IFFT may be used to create a complex OFDM signal in the baseband and expressed as:

$$x_n = \frac{1}{\sqrt{N}} \sum_{k=0}^{N-1} X_k \exp\left(\frac{2j\pi kn}{N}\right), \quad n = 0, 1, \ldots, N-1 \tag{13}$$

is shown in equation (13) [38]. The phenomenon of inter-symbol interference (ISI) resulting from multipath propagation affects the entire conventional wireless communication systems. A CP with a duration of $N_{CP}$ data sets samples is employed, which is introduced at the onset of the OFDM symbol via duplicating the final $N_{CP}$ samples obtained from the IFFT output $x_n$ and inserting them at the start of $x_n$, which aims to surpass the maximum dispersion delay of the fading channel $(L_d)$. As a result, the transmitted symbols $\tilde{x} = [x_{N-N_{CP}}, x_{N-N_{CP}+1}, \ldots, x_N, x_0, x_1, \ldots, x_{N-1}]$, are generated, which have a total length of $N_t = N + N_{cp}$ samples. This technique effectively reduces the influence of ISI that occurs between consecutive OFDM signals within channels. The aforementioned carriers traverse a diverse range of fading channels, whereby each channel introduces its own distinct noise at the point of reception. This noise contributes to the signal as shown in equation (14).

### 3.2. Multipath channel model

The assumption of some degree of noise distortion in transmitted signals is fundamental to the work of communication theory. In most cases, it is supposed that the noise is AWGN. A more practical situation for wireless communications is when transmitters and receivers may be connected via multiple paths. These paths may be straight or generated by processes including reflection, diffraction, and scattering. The gathered signal is a vector of individual delayed signals, each of which has its own frequency, amplitude, and delay [39].

For short-term or localized fades, the Rayleigh and Rician distributions are useful, but the lognormal distribution is better suited to explain longer-term or worldwide occurrences. On the other hand, Nakagami's m-distribution [40] is a more adaptable statistical model that can replicate both the Rayleigh and the

one-sided Gaussian fading scenarios. Furthermore, at certain intervals on the mean rating scale, the Nakagami distribution may serve as a suitable approximation to the Rician and log-normal distributions [38].

The Nakagami and Rician distributions are a better fit for low signal-to-noise levels (SNRs) than they are for high SNRs. The Nakagami distribution also gives a better fit to experimental data over a broad range of propagation in the physical channels, and it is more flexible than the log-normal and Rician distributions [38]. The performance of a system will suffer greatly if fading occurs.

The flat fading channel model is the one that is used the most often for limited bandwidth transmission via mobile and wireless channels. The flat fading channel reduces the strength of all of the individual frequency elements that make up the signal equally. Because of this, the received signal, which was in its complex baseband form, may be expressed as [41, 42]:

$$Y = \beta X + U, \tag{14}$$

where $Y$ represents the signal that was received and $X$ represents the symbol that was sent, $U$ is AWGN amplitude, and $\beta$ is the fading channel coefficients. A stochastic function is the amplitude of the fade, which is represented by the symbol "$\beta$" The channel exhibits nothing but AWGN when there is no fading at all ($\beta = 1$).

If the amplitude of the fading channel adheres to the Rayleigh distribution, then the probability distribution $P(|\beta|)$ may be written as the following [43]:

$$f_\beta(\beta) = \frac{\beta}{\sigma_h^2} \exp\left(-\frac{\beta^2}{2\sigma_h^2}\right). \tag{15}$$

In this situation, the in-phase and quadrature-phase components will both have distributions that are Gaussian with $N(0,\ 1/2)$ as:

$$f_\beta\left(\beta^I\right) = \frac{1}{\sqrt{2\pi\sigma_h^2}} \exp\left(-\frac{\left(\beta^I\right)^2}{2\sigma_h^2}\right), \quad -\infty \le \beta^I < \infty, \tag{16}$$

$$f_\beta\left(\beta^Q\right) = \frac{1}{\sqrt{2\pi\sigma_h^2}} \exp\left(-\frac{\left(\beta^Q\right)^2}{2\sigma_h^2}\right), \quad -\infty \le \beta^Q < \infty, \tag{17}$$

where $\sigma_h^2$ indicate the typical strength of the signal that was received, which is based on the path of loss and the shadowing alone.

The quality of the connection may be negatively impacted in terrestrial and satellite land-mobile systems by the gradual variation in the average mean signal strength that is brought on by the shadowing caused by topography, buildings, and trees. The performance of the communication system will only be dependent on the influence of shadowing if the radio receiver can mitigate the fast fluctuations caused by multipath fading via averaging, or if the impacts of multipath are mitigated by employing a reliable diversity network. Based on actual observations, there is widespread agreement that shadowing may be represented by log-normal distribution for a variety of situations, both indoors and outdoors [44–46]. In this scenario, the route SNR per symbol $\beta$ will have a probability density function (PDF) that is provided by the conventional log-normal equation. Consequently, the amplitude of the fading in the time domain follows the log-normal distribution and is described as:

$$f_\beta\left(\beta^\Upsilon\right) = \frac{\Lambda}{\beta^\Upsilon\sqrt{2\pi}\sigma} \exp\left(-\frac{\left(10\log_{10}\beta^\Upsilon - m\right)^2}{2\sigma^2}\right). \tag{18}$$

Equation (18), which can alternatively be represented as:

$$f_\beta\left(\beta^\Upsilon\right) = \frac{1}{\beta^\Upsilon\sqrt{2\pi\sigma^2}} \exp\left(-\frac{\left(\ln\beta^\Upsilon - m\right)^2}{2\sigma^2}\right), \tag{19}$$

where $0 \le \beta^\Upsilon < \infty$, and $\beta^\Upsilon > 0$, and $\Upsilon = \{I,\ Q\}$ indicate the real component and imaginary component, respectively.

The parameters $m$ and $\sigma$ represent the average mean and standard deviation of the logarithm of $\beta^\Upsilon$, respectively. It is possible to represent those parameters in $dB$, as $\sigma = \sigma_{\text{dB}}/\Lambda$ and $m = m_{\text{dB}}/\Lambda$, where the value $\Lambda = \frac{10}{\ln 10} = 4.3429$ [47]. The PDF of the variable in decibels will be Gaussian if the lognormal variable is changed to decibel units. One may represent the parameter $m$ in terms of average signal-to-noise ratio (SNR) in such a way $m_{\text{dB}} = \beta^\Upsilon - \frac{\sigma_{\text{dB}}^2}{\Lambda}$. For the majority of wireless network communication regimes over channel has log-normal distribution, the $\sigma_{\text{dB}}$ parameter, sometimes referred to as the dB spread, was observed to fluctuate within a certain range of 1–12 dB [48]. For the actual dB spread in mobile communication, Fig. 3 displays the PDF plot and the typical SNR ($\beta^\Upsilon$ dB). After performing an FFT function, the distribution of the channel real and imaginary parts in equations (18) or (19) will become increasingly closer to a normal distribution, as stated by the central limit theorem (CLT), i.e. $f_\beta\left(\beta^\Upsilon\right) = N(\beta^I, 0, \sigma_{LN}^2)$ and $f_\beta\left(\beta^\Upsilon\right) = N(\beta^Q, 0, \sigma_{LN}^2)$, where $\beta^I$ and $\beta^Q$ are zero-mean sta-

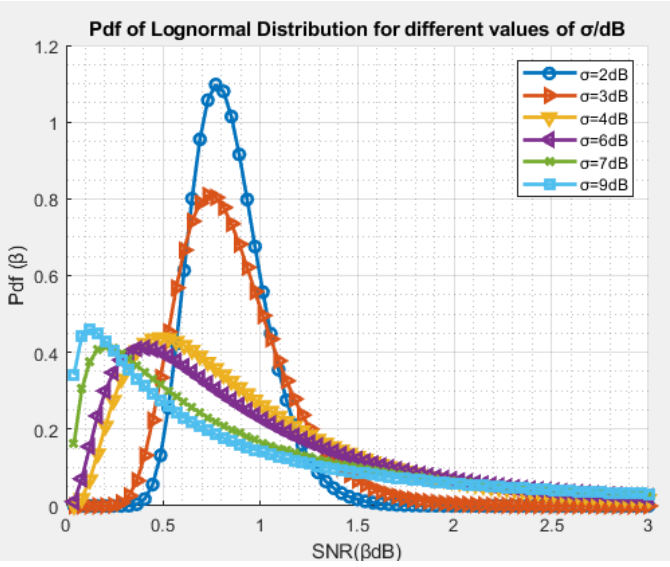


**Fig. 3.** PDF of an instantaneous SNR for different $\sigma$ dB values with $m$ dB = 1

tistically independent orthogonal Gaussian R.V. utilizing the value of equation (19) to determine the variance.

$$\sigma_{LN}^2 = E\left\{\left|\beta^{\Upsilon}\right|^2\right\} - \left(E\left\{\left|\beta^{\Upsilon}\right|\right\}\right)^2, \tag{20}$$

$$\sigma_{LN}^2 = \int_0^{\infty} (\beta^{\Upsilon})^2 f_{\beta}\left(\beta^{\Upsilon}\right) \mathrm{d}\beta^{\Upsilon} - \left(\int_0^{\infty} \beta^{\Upsilon} f_{\beta}\left(\beta^{\Upsilon}\right) \mathrm{d}\beta^{\Upsilon}\right)^2, \tag{21}$$

$$\sigma_{LN}^2 = \int_0^{\infty} \frac{\beta^{\Upsilon}}{\sqrt{2\pi\sigma^2}} \exp\left(-\frac{\left(\ln\left(\beta^{\Upsilon} - m\right)\right)^2}{2\sigma^2}\right) \mathrm{d}\beta^{\Upsilon} - \left(\int_0^{\infty} \frac{1}{\sqrt{2\pi\sigma^2}} \exp\left(-\frac{\left(\ln\left(\beta^{\Upsilon} - m\right)\right)^2}{2\sigma^2}\right) \mathrm{d}\beta^{\Upsilon}\right)^2. \tag{22}$$

Let $a = \dfrac{1}{\sqrt{2\pi\sigma^2}}$, $b = \dfrac{1}{2\sigma^2}$ and $\operatorname{erf}\left(\beta^{\Upsilon}\right) = \dfrac{2}{\sqrt{\pi}} \int_0^{\infty} e^{-z^2} \mathrm{d}z$

$$\sigma_{LN}^2 = \frac{\sqrt{\pi} a\, e^{\frac{1}{b}+2m}}{2\sqrt{b}} \operatorname{erf}\left(\frac{-bm + b\log(\beta) - 1}{\sqrt{b}}\right)\Bigg|_0^{\infty} - \left(\frac{\sqrt{\pi} a\, e^{\frac{1}{4b}+m}}{2\sqrt{b}} \operatorname{erf}\left(\frac{-2bm + b\log(\beta) - 1}{2\sqrt{b}}\right)\Bigg|_0^{\infty}\right)^2, \tag{23}$$

$$\sigma_{LN}^2 = \frac{\sqrt{\pi} a\, e^{\frac{1}{b}+2m}}{\sqrt{4b}} - \left(-\frac{\sqrt{\pi} a\, e^{\frac{1}{b}+2m}}{\sqrt{4b}}\right) - \left(\frac{\sqrt{\pi} a\, e^{\frac{1}{4b}+m}}{\sqrt{4b}} - \left(-\frac{\sqrt{\pi} a\, e^{\frac{1}{4b}+m}}{\sqrt{4b}}\right)\right)^2, \tag{24}$$

$$\sigma_{LN}^2 = \frac{\sqrt{\pi}\sqrt{2\sigma^2}}{\sqrt{2\pi\sigma^2}} e^{2\sigma^2+2m} - \left(\frac{\sqrt{\pi}\sqrt{2\sigma^2}}{\sqrt{2\pi\sigma^2}} e^{\frac{2\sigma^2}{4}+m}\right)^2, \tag{25}$$

$$\sigma_{LN}^2 = e^{2\sigma^2+2m} - \left(e^{\left(\frac{\sigma^2}{2}\right)+m}\right)^2, \tag{26}$$

$$\sigma_{LN}^2 = e^{2m}\left(e^{2\sigma^2} - e^{\sigma^2}\right). \tag{27}$$

### 3.3. Receiver

The extraction of $N_{cp}$ samples of OFDM carrier and then running an FFT operation will produce the received signal in the frequency domain. This mathematical operation facilitates the conversion of the signal of the frequency domain from the time domain to the frequency domain. Equation (14) represents the complex signal at the receiver, which may be represented in the frequency domain as follows:

$$Y^I + jY^Q = \left(Z^I + jZ^Q\right)\left(X^I + jX^Q\right) + U^I + jU^Q. \tag{28}$$

In the frequency domain, the symbols $Y$, $Z$, $X$, and $U$ represent the following entities: $Y$ denotes the complex signal, $Z$ represents the complex fading channel transfer function, $X$ stands for the complex modulated signals, and $U$ signifies the AWGN [39]. As per the CLT, the real component and the imaginary part distributions tend to approximate a Gaussian distribution subsequent to the FFT operation [49, 50]. The mean of these distributions is zero, but the variance is based on the specific channel used. In the context of Rayleigh fading channel, the PDF $(Z^I)$ and the PDF $(Z^Q)$ may be represented as (16) and (17). In the context of the lognormal fading channel, the probabilities $P(Z^I)$ and $P(Z^Q)$ may be mathematically represented as:

$$f_Z\left(Z^I\right) = \frac{1}{\sqrt{2\pi\sigma_{LN}^2}} \exp\left(-\frac{\left(Z^I\right)^2}{2\sigma_{LN}^2}\right), \quad 0 \le Z^I < \infty, \tag{29}$$

$$f_Z\left(Z^Q\right) = \frac{1}{\sqrt{2\pi\sigma_{LN}^2}} \exp\left(-\frac{\left(Z^Q\right)^2}{2\sigma_{LN}^2}\right), \quad 0 \le Z^Q < \infty, \tag{30}$$

where $\sigma_{LN}^2$ is the variance of the lognormal fading channel as previously derived equation (23). Therefore, it is evident the amplitude of the channel frequency response, denoted as $|Z|$, follows the Rayleigh distribution in the frequency response for previous channels. This may be mathematically represented as $|Z| = \sqrt{\left(Z^I\right)^2 + \left(Z^Q\right)^2}$.

When ISI is greater than noise, the ZF equalizer linear technique inverts the frequency response of that channel to recover the transmitted signal. Consequently, the signal received in equation (28) may be equalized by performing division on both sides of that equation using $(1/H)$. In an M-QAM scheme, the received signal that is complex and noisy is represented as Y in the frequency domain, while the collection of all feasible modulated symbols $X$ is indicated as $C$, where $C = \{C_1, C_2, C_3, \ldots, C_M\}$. Finally, the decoding algorithm of NR-LDPC codes is suggested to be accomplished by the use of adaptive LMS decoding techniques. To enhance the precision of the soft bits that are sent throughout the iterative decoding process in equation (11).

The BER in the AWGN may be expressed as:

$$P_b^{AWGN} = \frac{1}{2} erfc\left(\sqrt{\frac{E_b}{No}}\right). \tag{31}$$

If $M$ is the square number and $M = 2^k$, then the BER for M-QAM is:

$$P_b^{AWGN} = \frac{1}{\log_2\sqrt{M}} \sum_{1}^{\log_2\sqrt{M}} P_b(k), \tag{32}$$

where [51]

$$P_b(k) = \frac{1}{\sqrt{M}} \sum_{i=0}^{(1-2^{-k})\sqrt{M}-1} \left[(-1)^{\left\lfloor \frac{i.2^{k-1}}{\sqrt{M}} \right\rfloor} \cdot \left(2^{k-1} - \frac{i.2^{k-1}}{\sqrt{M}} - 1\right) \cdot \operatorname{erfc}\left((2.i+1)\sqrt{\frac{3(\log_2 M).r}{2(M-1)}}\right)\right]. \tag{33}$$

Expanding $P_b(k)$ is possible at $i = 1, 2, \ldots, \left(1-2^{-k}\right).\sqrt{M} - 1$. To achieve increased efficiency,

$$P_{b(64QAM)}^{AWGN} = \frac{7}{12} Q\left(\sqrt{\frac{2E_b}{N_0}}\right). \tag{34}$$

Equation (34) can be expressed in terms of erfc( ) as

$$P_{b(64QAM)}^{AWGN} = \frac{7}{24}\text{erfc}\left(\sqrt{\frac{E_b}{7No}}\right), \tag{35}$$

$$P_{b(256QAM)}^{AWGN} = \frac{15}{64}\text{erfc}\left(\sqrt{\frac{4E_b}{85No}}\right). \tag{36}$$

## 4. BER COMPUTATION OVER LOG-NORMAL CHANNEL

To estimate the BER in AWGN for the QAM-OFDM system under the impact of log-normal fading channel, the ratio of actual bit energy to noise is $SNR = \beta_b = \frac{|Z|^2 E_b}{N_0}$ Consequently, for a certain value of $Z$, the bit error conditional probability is:

$$P_{b|Z} = \frac{1}{2}\text{erfc}\left(\sqrt{\beta_b}\right). \tag{37}$$

Based on our analysis of the chi-square random variable, it can be inferred that a Rayleigh distributed random variable has two degrees of freedom, and can be expressed as:

$$p\left(\beta_b\right) = \frac{1}{E_b/2\sigma_u^2} e^{\frac{\beta_b}{E_b/2\sigma_u^2}}, \quad \beta_b \geq 0, \tag{38}$$

$$P_b^{\text{Log-normal}} = \int_0^\infty \frac{1}{2} erfc\left(\sqrt{\beta_b}\right) p\left(\beta_b\right) \mathrm{d}\beta_b$$

$$= \int_0^\infty \frac{1}{2}\text{erfc}\left(\sqrt{\beta_b}\right) \frac{1}{E_b/2\sigma_u^2} e^{\frac{\beta_b}{E_b/2\sigma_u^2}} \mathrm{d}\beta_b,$$

$$P_b^{\text{Log-normal}} = \frac{1}{2}\left[1 - \left(\frac{\sqrt{\sigma_{LN}^2 \frac{E_b}{2\sigma_u^2}}}{\sqrt{1+\sigma_{LN}^2 \frac{E_b}{2\sigma_u^2}}}\right)\right]. \tag{39}$$

## 5. NUMERICAL SIMULATION AND PERFORMANCE

The focus of this research is to assess a proposed system performance NR-LDPC-QAM-OFDM in terms of BER across communication channels. Specifically, we investigate the lognormal fading channel. The suggested system performance assessment is compared to that of an uncoded QAM-OFDM system. Figure 4 presents a comparison process of BER performance between $BG1$ and $BG2$ for LDPC code. The initial coding rates were set at 1/2 for two distinct block lengths, specifically 3840 and 4928. And later they were fixed at (1/3) for the identical code lengths. The BER results of the two systems are compared with the results of a Monte Carlo simulation and a theoretically determined BER that was calculated using equation (28). It can be shown in Fig. 4 that the $BG1$-NR-LDPC-COFDM outperforms the $BG2$-NR-LDPC COFDM LDPC-COFDM for long block length by 0.95 dB at BER = $10^{-5}$, in the scenario when the rate is 1/3 and provides coding gain about 11.4 dB compared to uncoded QAM–OFDM scheme.

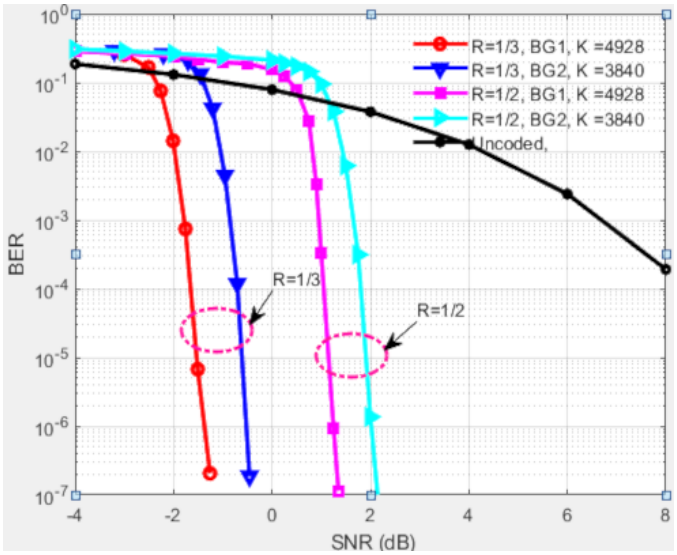


**Fig. 4.** BER of LDPC-COFDM for two scenarios with AWGN

When employing different modulation techniques, Fig. 5 demonstrates the BER vs. SNR curve for a message consisting of 4928 bits. While the modulation methods are performed, 4QAM, 16QAM, 64QAM, 256QAM, and 1024QAM are supported. The findings obtained indicate that the 4QAM modulation technique exhibits superior performance when compared to the conducted simulations.

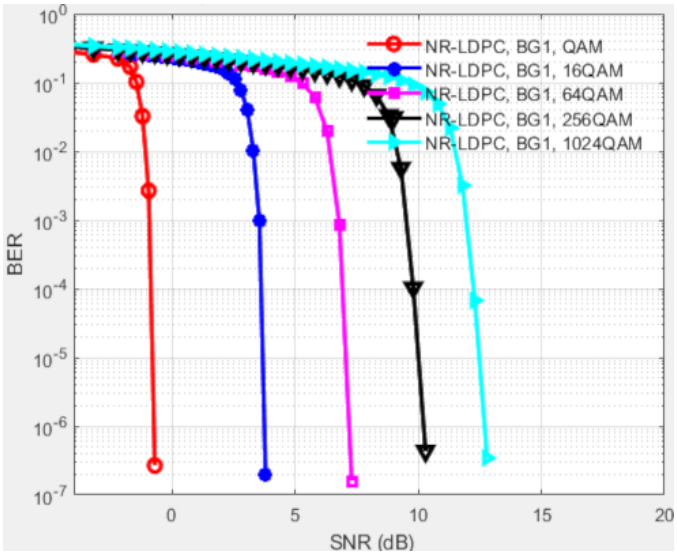


**Fig. 5.** BER of LDPC-COFDM system-based scenarios involving M-QAM with AWGN

The estimation of variances in the AWGN channel model is carried out by utilizing SNR measurements. The AWGN channel block that was employed previously accompanied a fading channel block in the presence of a fading scenario.

Figures 6 and 7 illustrate the performance analysis of the NR-LDPC-QAM-OFDM system for $BG1$ at both code rates (1/2, and 1/3), in comparison to the performance of the UOFDM technique in terms of BER, under the influence of a lognormal

fading channel. In contrast to SPA and MSA, the layered MS technique was used for decoding, and success was achieved with fewer iterations.

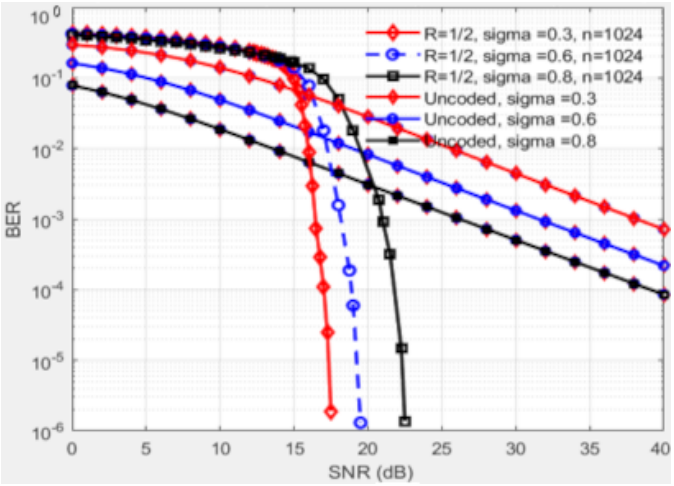


**Fig. 6.** BER of NR- LDPC-COFDM-QAM systems over the lognormal fading channel for BG1 at R = 1/2

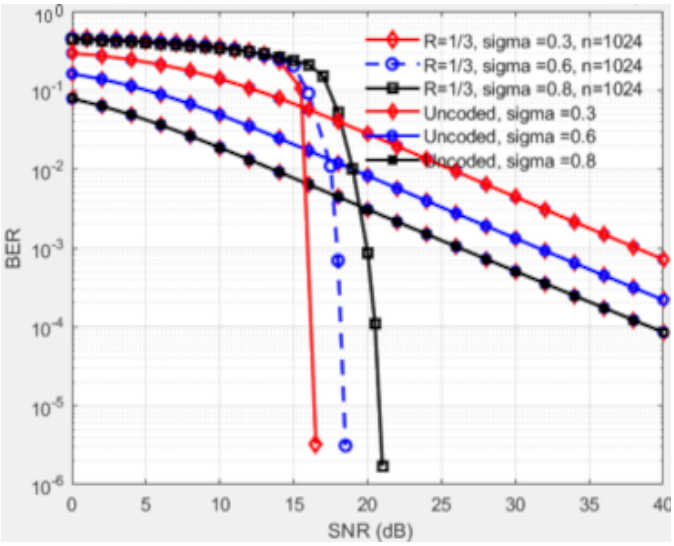


**Fig. 7.** BER of NR-LDPC-COFDM-QAM systems over the lognormal fading channel for BG1 at R = 1/3

The performance analysis of the NR-LDPC Code-QAM-OFDM proposed system, including both rates (1/2 and 1/3), for *BG*2 is illustrated in Figs. 8 and 9, and the system performance under the impact of a lognormal fading channel is shown in these figures. The results of this analysis are evaluated in relation to the UOFDM system performance under different values of sigma.

The simulation demonstrates a close alignment between the theoretical BER and the real BER for Uncoded OFDM across a lognormal channel fading scenario. It is evident that within the lower SNR range of 0 to 10.5 dB, the systems using NR-LDPC codes exhibit worse performance compared to those without any coding scheme. This is justified by the fact that the SNR is low

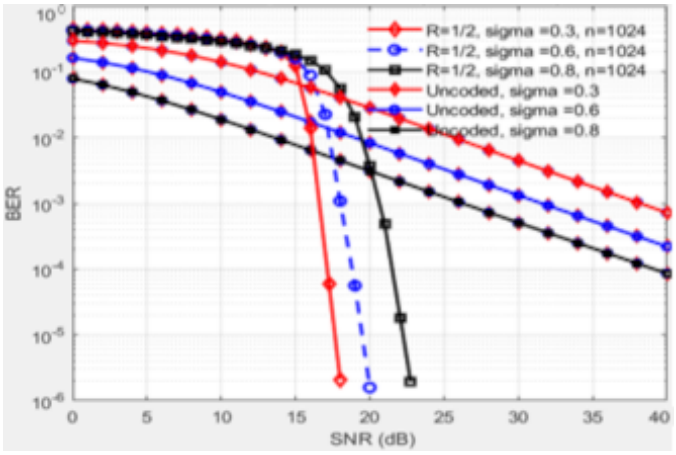


**Fig. 8.** ER of NR-LDPC-COFDM systems over the lognormal fading channel for BG2 at R = 1/2

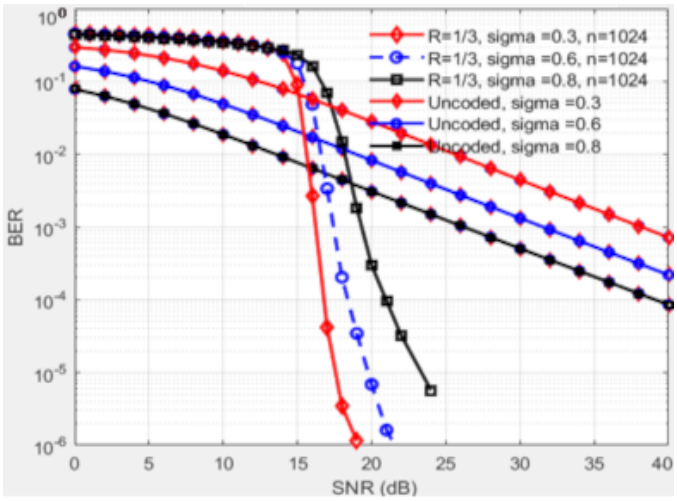


**Fig. 9.** BER of NR-LDPC-COFDM system over the lognormal fading channel for BG2 at R = 1/3

enough, yielding a rather high rate of error. Consequently, attempting error correction would be counterproductive. However, the performance of average BER in QAM -OFDM systems was significantly enhanced in the higher SNR area by utilizing LDPC codes.

Our findings clearly confirm the effectiveness of the newly constructed layered min-sum detector, as shown in Fig. 1. Comparative investigations show that this detector outperforms traditional approaches, especially in lognormal fading conditions seen in urban and suburban environments. The use of a developed layered method enables more efficient processing and improved error correction, resulting in a significant boost in system performance. Results shown in the simulation reveal a significant drop in bit error rates when compared to the standard models, indicating the improved capabilities of our novel detection approach.

A tabular comparison is presented, summarizing the stated investigations based on the kind of decoder, the BER with SNR, code gain, and modulation type described in Table 1.

**Table 1**
Comparison results of different publications

| Reference | Channel model | Decoder | BER/FER vs SNR | Modulation |
|---|---|---|---|---|
| [52] | AWGN | LDPC (min-sum) | 0.096173 at 1 dB | BPSK |
| [2] | AWGN | LDPC (sum product) | $10^{-4}$ at 1 dB | QPSK |
| [53] | Flat Rayleigh fading with CSI TR | LDPC(EXIT) | $10^{-4}$ at −0.7 dB | 16QAM (Anti-gray) |
| [53] | Flat Rayleigh fading with CSI TR | LDPC(EXIT) | $10^{-4}$ at −0.32 dB | 16QAM (Gray) |
| [54] | AWGN | LDPC(BP-OSD) | $10^{-4}$ at 5 dB | – |
| [38] | Rayleigh fading | LMS | $10^{-4}$ at 9 dB | QAM-OFDM |
| [38] | Nakagami-m | LMS | $10^{-4}$ at 7 dB | QAM-OFDM |

## 6. CONCLUSIONS

The multipath fading channel is taken into account in this research while evaluating how well the NR- LDPC- OFDM system performs. The lognormal fading channel is used to include the many phenomena that lead to signal distortion inside the channel. Employing Monte Carlo simulations, we observed that the QAM constellation in an NR-LDPC-COFDM was enhanced in terms of coding gain in comparison to the uncoded OFDM system. This improvement is achieved by using the log-likelihood ratio (LLR) calculated from the PDFs of the noise created at the output of the zero-forcing (ZF) equalizer in the fading scenario of channels. Moreover, it was shown that the LDPC-COFDM system, when combined with LMS decoding techniques, had superior performance compared to other algorithms.

In simulations of the QAM-NR-LDPC-COFDM system operating in AWGN over the LFC, a range of standard deviations (sigma = 0.3, 0.6, and 0.8) were evaluated, the findings demonstrate that for higher values of SNR, the LFC has better coding gain than the other fading channels as sigma decreases. For example, it can be seen that the use of the proposed QAM-LDPC-OFDM when applying BG1 leads to a coding gain of about 23.1 dB and 22.3 at a rate (1/3) and rate (1/2) respectively, higher than that of uncoded OFDM, considering BER of around $10^{-3}$ in the case of (sigma = 0.3). In addition, the use of the LMS decoding algorithm significantly decreases the BER of the system. In the end, it is found that NR-LDPC code can improve the system BER performance in the multipath fading channel. Therefore, To get a BER of $10^{-6}$, it is necessary to use LDPC code with LMS technique decoding.

## REFERENCES

[1] W. Ji, Z. Wu, K. Zheng, L. Zhao, and Y. Liu, "Design and Implementation of a 5G NR System Based on LDPC in Open Source SDR," in *2018 IEEE Globecom Workshops (GC Wkshps)*, Abu Dhabi, United Arab Emirates, 2018, pp. 1–6, doi: 10.1109/GLOCOMW.2018.8644263.

[2] T. Richardson and S. Kudekar, "Design of Low-Density Parity Check Codes for 5G New Radio," *IEEE Commun. Mag.*, vol. 56, no. 3, pp. 28–34, March 2018, doi: 10.1109/ MCOM. 2018. 1700839.

[3] R.G. Gallager, "Low-density parity-check codes," *IRE Trans. Inf. Theory*, vol. 8, no. 1, pp. 21–28, Jan. 1962.

[4] W.E. Ryan, "An introduction to LDPC codes," in *CRC Handbook for Coding and Signal Processing for Magnetic Recording Systems*, B. Vasic, Ed., Boca Raton, FL, USA: CRC Press, 2004, Ch. 36.

[5] Y. Fang, G. Bi, Y.L. Guan, and F.C.M. Lau, "A Survey on Protograph LDPC Codes and Their Applications," *IEEE Commun. Surv. Tutor.*, vol. 17, no. 4, pp. 1989–2016, 2015, doi: 10.1109/COMST. 2015.2436705.

[6] IEEE Standard for Information Technology–Telecommunications and Information Exchange between Systems – Local and Metropolitan Area Networks–Specific Requirements, "Part 11: Wireless LAN Medium Access Control (MAC) and Physical Layer (PHY) Specifications," Redline," IEEE Std 802.11-2020, pp. 1–767, 26 Feb. 2021, doi: 10.1109/IEEESTD.2021.9363693.

[7] Advanced Television Systems Committee, ATSC Standard : Physical Layer Protocol (A/322), 2018.

[8] ETSI – EN 302755, "Digital Video Broadcasting (DVB); Frame structure channel coding and modulation for a second generation Digital Terrestrial Television Broadcasting System (DVB-T2)," pp. 1–188, Jul., 2015.

[9] J. Song *et al.*, "Key technologies and measurements for DTMB – A system," *IEEE Trans. Broadcast.*, vol. 65, pp. 53–64, Mar. 2019.

[10] J. Malhotra, "Investigation of Channel Coding Techniques for High Data Rate Mobile Wireless Systems," *Int. J. Comput. Appl.,* vol. 115, no. 3, pp. 39–45, 2015.

[11] W. Sułek, "The design of structured LDPC codes with algorithmic graph construction," *Bull. Pol. Acad. Sci. Tech. Sci.*,vol. 70, no. 4, pp. 1–8, 2022, doi: 10.24425/bpasts.2022.141592.

[12] R. Hema, A. Ananthi, and D.C. Diana, "Coded GFDM with decision feedback equaliser for enhanced perform ance in underwater wireless optical communication," *Opto-Electronics Review*, vol. 32, no.1, p. 148697, 2024. doi: 10.24425/opelre.2024.148697.

[13] G.A. Al-rubaye, C.C. Tsimenidis, and M. Johnston, "Performance evaluation of T-COFDM under combined noise in PLC with log-normal channel gain using exact derived noise distributions," *IET Commun.*, vol. 13, no. 6, pp. 766–775, 2019, doi: 10.1049/iet-com.2018.6185.

[14] D.S. Shafiullah, M.R. Islam, M. Mostafa, A. Faisal, and I. Rahman, "Optimized Min-Sum decoding algorithm for Low Density PC codes," *2012 14th International Conference on Advanced Communication Technology (ICACT)*, 2012, pp. 475–480.

[15] W. Zhou and M. Lentmaier, "Generalized Two-Magnitude Check Node Updating with Self Correction for 5G LDPC Codes Decoding," *SCC 2019; 12th International ITG Conference on Systems, Communications and Coding*, Rostock, Germany, 2019, pp. 1–6, doi: 10.30420/454862047.

[16] M.K. Roberts and R.A. Jayabalan, "Modified Optimally Quantized Offset Min-Sum Decoding Algorithm for Low-Complexity LDPC Decoder," *Wirel. Pers Commun.*, vol. 80, pp. 561–570, 2015, doi: 10. 1007/s11277-014-2026-2.

[17] D.D. Kumar and R.S. Selvakumari, "Performance analysis of Min-Sum based LDPC decoder architecture for 5G new radio standards," *Mater. Today-Proc.*, vol. 62, pp. 4965–4972, 2022, doi: 10.1016/j.matpr.2022.03.693.

[18] K. Sun and M. Jiang, "A Hybrid Decoding Algorithm for Low-Rate LDPC codes in 5G," *2018 10th International Conference on Wireless Communications and Signal Processing (WCSP)*, Hangzhou, China, 2018, pp. 1–5, doi: 10.1109/WCSP.2018.8555597.

[19] X. Wu, M. Jiang, and C. Zhao, "Decoding optimization for 5G LDPC codes by machine Learning," *IEEE Access*, vol. 6, pp. 50179–50186, 2018.

[20] S. Enoch and I. Otung, "Performance Improvements in SNR of a Multipath Channel Using OFDM-MIMO," *Int. J. Electron. Telecommun.*, vol. 69, no. 4, pp. 769–773, 2023, doi: 10.24425/ijet.2023.147700.

[21] M.H. Ali and G.A. Al-Rubaye, "Performance Evaluation of 5G New Radio Polar Code over Different Multipath Fading Channel Models," *Int. J. Intell. Eng. Syst.*, vol. 17, no. 2, pp. 439–452, 2024, doi: 10.22266/ijies2024.0430.36.

[22] N. Narayana, and P. Sure, "Performance of a Software Defined Radio based Non-Coherent OFDM Wireless Link ," *Int. J. Electron. Telecommun.*, vol. 69, no. 3, pp. 537–544, 2023, doi: 10.24425/ijet.2023.146504.

[23] Z. Yu, T. Lu, W. Zheng, H. Feng Z. Ma, and F. Zhu, "Novel memory efficient LDPC decoders for beyond 5G," *Phys.Commun.*, vol. 51, p. 101538, 2022, doi: 10.1016/j.phycom.2021.101538.

[24] V. Vasylenko, S. Zaitsev, Y. Tkach, O. Korchenko, R. Ziubina, and O. Veselska, "Method of assessing the information reliability of in 5G wireless transmission systems," *Int. J. Electron. Telecommun.*, vol. 70, no. 1, pp. 205–210, 2024, doi: 10.24425/ijet.2024.149532.

[25] C. Zhang, X. Mu, J. Yuan, H. Li, and B. Bai, "Construction of Multi-Rate Quasi-Cyclic LDPC Codes for Satellite Communications," *IEEE Trans. Commun.*, vol. 69, no. 11, pp. 7154–7166, Nov. 2021, doi: 10.1109/TCOMM.2021.3107578.

[26] F. Hamidi-Sepehr, A. Nimbalker, and G. Ermolaev, "Analysis of 5G LDPC Codes Rate-Matching Design," *IEEE 87th Vehicular Technology Conference (VTC Spring)*, Porto, Portugal, 2018, pp. 1–5, doi: 10.1109/VTCSpring.2018.8417496.

[27] Multiplexing and Channel Coding, document TS 38.212 V15.0.0, 3GPP, Dec. 2018.

[28] M. Soszka, "Fading Channel Prediction for 5G and 6G Mobile," *Int. J. Electron. Telecommun.*, vol. 68, no. 1, pp. 153–160, 2022, doi: 10.24425/ijet.2022.139863.

[29] V.L. Petrović, D.M. El Mezeni, and A. Radošević, "Flexible 5g new radio ldpc encoder optimized for high hardware usage efficiency," *Electronics*, vol. 10, no. 9, 2021, doi: 10.3390/electronics10091106.

[30] O. Bancalo. G. Kolm Ban, D. Declercq, and V. Savin, "Code-design density for efficient layered LDPC decoders with bank memory organization," *Microproces. Microsyst.*, vol. 63, pp. 216–225, Nov. 2018, doi: 10.1016/j.micpro.2018.09.011.

[31] T. Thi, B. Nguyen, T.N. Tan, and H. Lee, "Efficient QC-LDPC Encoder for 5G New Radio," *Electronics*, vol.8, no. 6, pp. 1–15, 2019, doi: 10.3390/electronics8060668.

[32] H. Cui, F. Ghaffari, K. Le, D. Declercq, J. Lin, and Z. Wang, "Design of High-Performance and Area-Efficient Decoder for 5G LDPC Codes," *IEEE Trans. Circ. Syst. I*, vol. 68, no. 2, pp. 879–891, Feb. 2021, doi: 10.1109/TCSI.2020.3038887.

[33] Y. Wang, M. Jiang and X. Ma, "Transmitting Extra Bits With Cyclically Shifted LDPC Codes," *IEEE Wirel. Commun. Lett.*, vol. 10, no. 12, pp. 2824–2827, Dec. 2021, doi: 10.1109/LWC.2021.3118675.

[34] J.V. Wonterghem, A. Alloum, J.J. Boutros, and M. Moeneclaey, "On short-length error-correcting codes for 5G-NR," *Ad Hoc Netw.*, vol. 79, pp. 53–62, 2018, doi: 10.1016/j.adhoc.2018.06.005.

[35] J. Xie., L. Yin, N. Ge, and J. Lu. "Improved layered min-sum decoding algorithm for low-density parity check codes," *9th WSEAS international conference on multimedia systems & signal processing*, 2009, pp. 102–107.

[36] J. Nadal and A. Baghdadi, "Parallel and Flexible 5G LDPC Decoder Architecture Targeting FPGA," *IEEE Trans. Very Large Scale Integr. (VLSI) Syst.*, vol. 29, no. 6, pp. 1141–1151, Jun. 2021, doi: 10.1109/TVLSI.2021.3072866.

[37] N. Kumar, D. Kedia, and G. Purohit, "A review of channel coding schemes in the 5G standard," *Telecommun. Syst.,* vol. 83, pp. 423–448, 2023, doi: 10.1007/s11235-023-01028-y.

[38] M.H. Ali and G.A. Al-Rubaye "Performance Analysis of 5G New Radio LDPC over Different Multipath Fading Channel Models," *Int. J. Comput. Netw. Inf. Secur.*, vol. 15, no. 4, pp. 1–12, 2023, doi: 10.5815/ijcnis.2023.04.01.

[39] H. Zarrinkoub, *Understanding LTE with MATLAB: from mathematical foundation to simulation, performance evaluation and implementation*, John Wiley & Sons, Ltd, 2014.

[40] M. Nakagami. "The m-distribution – A General Formula of Intensity Distribution of Rapid Fading," in *W.C. Hoffman: Statistical Methods of Radio Wave Propagation*, 1960, pp. 3–36, doi: 10.1016/B978-0-08-009306-2.50005-4.

[41] D.V. Ha, T.T. Huong, and N.T. Hai, "Performance Investigation of High-Speed Train OFDM Systems under the Geometry-Based Channel Model," *Int. J. Electron. Telecommun.*, vol. 67, no. 3, pp. 451–457, 2021, doi: 10.24425/ijet.2021.137833.V.

[42] G.A. Al-rubaye, "Performance of 5G NR-polar QAM-OFDM in nonlinear distortion plus Non-Gaussian noise over Rayleigh fading channel," *AEUE-Int. J. Electron. Commun.*, vol. 171, p. 154929, 2023, doi: 10.1016/j.aeue.2023.154929.

[43] C. Xiao, Y.R. Zheng, and N.C. Beaulieu, "Statistical simulation models for Rayleigh and Rician fading," *IEEE International Conference on Communications, 2003. ICC '03*, Anchorage, USA, 2003, vol. 5, pp. 3524–3529, doi: 10.1109/ICC.2003.1204109.

[44] N. Quoc-tuan, D. Nguyen, and L.S. Cong, "A 10-state model for an AMC scheme with repetition coding in mobile wireless networks," *J. Wirel. Commun. Netw.*, vol. 2013, p. 219, Sep. 2013. doi: 10.1186/1687-1499-2013-219.

[45] H. Suzuki, "A statistical model for urban radio propagation," *IEEE Trans. Commun.*, vol. 25, no. 7, pp. 673–680, Jul. 1977, doi: 10.1109/TCOM.1977.1093888.

[46] M.K. Simon, *Digital Communication over Fading Channel, 2nd Ed.*, John Wiley & Sons, INC. Publication, 2005.

[47] A. Laourine, A. Stephenne, and S. Affes, "On the capacity of log-normal fading channels," *IEEE Trans. Commun.*, vol. 57, no. 6, pp. 1603–1607, Jun. 2009, doi: 10.1109/TCOMM.2009.06.070109.

[48] F. Heliot, X. Chu, R. Hoshyar, and R. Tafazolli, "A tight closed-form approximation of the log-normal fading channel capacity," *IEEE Trans. Wirel. Commun.*, vol. 8, no. 6, pp. 2842–2847, June 2009, doi: 10.1109/TWC.2009.080972.

[49] P. McCullagh, "Gaussian Distributions," in *Ten Projects in Applied Statistics, Springer Series in Statistics*, P. Bühlmann, P. Diggle, U. Gather, and S. Zeger, Eds., Springer, Cham, 2023, pp. 251–277, doi: 10.1007/978-3-031-14275-8_15.

[50] B. Tahir, S. Schwarz and M. Rupp, "BER comparison between Convolutional, Turbo, LDPC, and Polar codes," *24th International Conference on Telecommunications (ICT)*, Limassol, Cyprus, 2017, pp. 1–7, doi: 10.1109/ICT.2017.7998249.

[51] J. Lu, K.B. Letaief, J.C.-I. Chuang, and M.L. Liou, "M-PSK and M-QAM BER computation using signal-space concepts," *IEEE Trans. Commun.*, vol. 47, no. 2, pp. 181–184, Feb. 1999, doi: 10.1109/26.752121.

[52] D. Dinesh and R.S. Selvakumari, "Performance analysis of Min-Sum based LDPC decoder architecture for 5G new radio standards," *Mater. Today-Proc.*, vol. 62, pp. 4965–4972, 2022, doi: 10.1016/j.matpr.2022.03.693.

[53] Y. Jiang, A. Ashikhmin, and N. Sharma, "LDPC Codes for Flat Rayleigh Fading Channels with Channel Side Information," *IEEE Trans. Commun.*, vol. 56, no. 8, pp. 1207–1213, 2008, doi: 10.1109/TCOMM.2008. 041040.

[54] L. Li, J. Xu, J. Xu, and L. Hu, "LDPC design for 5G NR URLLC & mMTC," in *Proc. IEEE International Conference on Communications*, 2020, pp. 1071–1076, doi: 10.1109/ ICC40277.2020.9148876.